

# **Application of an End-User Friendly Cryogenic Coil For In Vivo High Resolution Medical Image on 3T Whole Body Scanner**

## **A novel liquid nitrogen cryostat and coil for high-resolution *in-vivo* imaging on a 3 tesla whole body scanner.**

Bobo Hu<sup>1</sup>, Gopal Varma<sup>2</sup>, Chris Randell<sup>3</sup>, Stephen Keevil<sup>2</sup>, Tobias Schaeffter<sup>2</sup> and Paul Glover<sup>1</sup>

<sup>1</sup>Sir Peter Mansfield Magnetic Resonance Centre, University of Nottingham, Nottingham; <sup>2</sup> St Thomas's Hospital, Kings College, London; <sup>3</sup>Pulseteq Ltd., Wotton-under-Edge, Gloucestershire.

### **Abstract:**

The design and operation of a receive-only liquid nitrogen (LN<sub>2</sub>) cooled coil and cryostat suitable for medical image on 3T whole body MR scanner is presented. The coil size, optimised for murine imaging, was determined by using electromagnetic (EM) simulations. This process is therefore easier and more cost-effective than building a range of coils. A non-magnetic cryostat suitable for small animal imaging was developed having a good vacuum and cryogenic temperature performance. The cooled probe had an active detuning circuit allowing use with the scanner's built-in body coil. External tuning and matching was adopted to allow for changes to the coil due to temperature and loading. The performance of the probe was evaluated by comparison of signal-to-noise (SNR) performance with the same radio-frequency (RF) coil operating at room temperature (RT). The performance of the RF coil at RT was also benchmarked against a commercial surface coil with similar dimensions to ensure a fair SNR comparison. The cryogenic coil achieved a 1.6 - 2 fold SNR gain for several different medical image applications: For the mouse brain image, a 100 µm resolution was achieved in an imaging time of 3 minutes with an SNR of 25-40, revealing finer anatomical details unseen at lower resolution in the same time. For other heavy loading condition, such as hind legs and liver, the SNR enhancement was slightly reduced to 1.6 fold. The observed SNR was in good agreement with the expected SNR gain correlated to the loaded quality factor of RF coils from EM simulations. With the aid of this end-user friendly and economically attractive cryogenic RF coil, the enhanced SNR available can be used to improve resolution or reduce time of individual scans in a number of biomedical applications.

## **Introduction:**

With the development of high field MRI, there is an increasing interest in and demand for investigating physiological and pathological models of small rodents on high field whole body MR scanners widely available in clinics [1]. One significant major obstacle in performing high resolution imaging on small rodents is the low signal to noise ratio (SNR) resulting from the small voxel size approaching the micron scale [2]. To improve the SNR, the resistance associated with the RF receiver hardware can be minimized by lowering its temperature and reducing the resistive loss of noise voltage [3]. The cryogenic probe approach therefore becomes an effective technique in achieving better SNR.

Several MRI applications of cryogenic coils have demonstrated good SNR performance compared with conventional RF coils performed at room temperature (RT). A 1.2 cm high temperature superconducting (HTS) coil has been utilised in mouse image on a 1.5 T whole body scanner [1]. Another group adopted a miniature volume HTS probe in a 9.4T small bore system to image *in vitro* mouse brain [4]. Such comparisons of HTS probes with copper coils at RT demonstrate SNR gains ranging from two to four times. The technical problems associated with such HTS coils [5] have appeared to limit the adoption of reliable HTS coils for *in-vivo* medical images [6]. On the other hand, cooling a normal copper coil to cryogenic temperature (CT) can greatly reduce its resistance and increase its quality factor by a two-fold [2]. Therefore the cryogenic copper coil becomes an attractive alternative to HTS coils due to its advantages in simplicity, ease of fabrication, stability and cost. A conventional copper coil cooled down by liquid helium to 30K has achieved a two-fold SNR gain of mouse brain images [7]. Wright, et al. developed a 17 mm copper surface coil with an upright liquid nitrogen (LN<sub>2</sub>) dewar cooling system at 1.5T field strength, and it achieved a factor of 2 improvement in SNR for *in-vivo* images of human fingers [2]. However, to date, low temperature detection devices have not been widely used for *in-vivo* medical imaging applications on high field whole body MR scanners, in spite of their success in low field MRI systems ranging from 0.2T to 1.5T [8].

There are a number of practical difficulties of applying such cryogenic probes for *in-vivo* medical images. First of all, the position of cryogenic coil relative to the sample is usually more than 3-4 mm away due to the thickness of insulation and/or vacuum required for the cooling device [2,7 & 9]. In many reports of implementation of cryo-coils there is no rigorous SNR comparison of the cryogenic coil against an optimized microscopy coil with similar size and suitable for similar

MRI/MRS applications. Therefore there has always been a long-standing suspicion that the benefit of adopting such device for MR imaging is very limited because of the increased coil-to-sample distance. Secondly, most cryostat designs are featured with an upside down cold head to improve thermal transfer to the RF coil [2 and 9]. This design creates difficulties of constructing suitable platforms for *in-vivo* samples, plus positioning and handling these samples with flexibility, and monitoring their physiological condition with ease. Thirdly, since most cryogenic probe-heads are designed as small surface coils with radii  $\leq 2$  cm [10], it is desirable to employ another transmitter to provide a homogenous  $B_1$  field and achieve the designed flip angle while utilizing the cryogenic coil as a highly sensitive receiver [1],[7]. Finally, up-to now, cryogenic probes have been only accessible to a few research groups due to the complexity of instrumentation. Therefore there are issues of applying cryogenic probe techniques to the multi-disciplinary applications beyond demonstration purposes [11].

In this work a novel copper coil at CT (CT-Copper) setup has been designed and optimised to address the above challenges associated with cryogenic coil applications for medical imaging. The coil size has been carefully chosen by a computational electromagnetic (EM) simulation to achieve the best SNR performance for murine imaging. An optimized circuit has been developed to actively decouple the cryogenic coil during transmission and which offers flexible matching capability after the cooling period and placement of the sample. A non-magnetic cryostat for  $LN_2$  coolant has been designed and constructed to achieve a balance between the good vacuum insulation and a stable low temperature. This cryostat successfully solved several problems associated with conventional cryostats, such as difficulty in handling and monitoring small animals and the big liftoff between sample and coil. The performance of this coil has been rigorously compared with its identical counterpart at RT (RT-Copper coil) for three different *in vivo* medical imaging applications (brain, leg and liver images) by using a whole body 3T MR scanner. The RT-copper coil performance has also been characterised against a commercially available 23 mm microscopy coil to ensure fair SNR comparisons. Several standard medical image protocols used with a clinical scanner and relevant to murine imaging were also tested in this work to demonstrate the ease of use, the signal gains and the stable performance of such setup.

## **Material and Methods:**

## (1) Theoretical Background and Simulation Study

The SNR for an elementary encoded volume (voxel)  $V_0$  carrying a transverse magnetization component  $M_T$  can be expressed as [12]:

$$SNR \approx F^{-1/2} S_{RF} V_0 M_T \sqrt{t_0/t_R} \sqrt{t_{scan}} \quad (1)$$

where the noise factor  $F$  accounts for the noise power introduced by the MR scanner electronics, and is normally close to unity [5]. The sampling window duration  $t_0$ , the repetition time  $t_R$  and the total scan time  $t_{scan}$  are filtering and averaging time parameters usually involved in scanning sequences and in Fourier reconstruction techniques [13].  $S_{RF}$  is the RF sensitivity factor which contributes to the SNR of an image as:

$$S_{RF} \approx (B_1/I) / \sqrt{R_{eq} T_{eq}} \quad (2)$$

where  $B_1/I$  is the magnetic flux density in the receiver coil induced by a unit current,  $R_{eq}$  is the equivalent total resistance, and  $T_{eq}$  is the equivalent operational temperature. In eqn. (2),  $R_{eq} T_{eq}$  can be replaced as the sum of a coil resistance contribution and a magnetically coupled sample contribution as:

$$R_{eq} T_{eq} = R_{coil} T_{coil} + R_{sample} T_{sample} \quad (3)$$

When both  $R_{sample}$  and  $R_{coil}$  are considered, the optimum coil size to achieve the best SNR is bigger than that obtained with only  $R_{sample}$  being considered. This is because the relative increase in coil loss for the smaller coil erodes the SNR advantage of further reductions in coil radius [14]. Since  $S_{RF}$  represents the time-domain SNR available from the RF coil per unit of magnetic moment and unit bandwidth, it is a direct measurement of the RF coil quality and its contribution to the overall image SNR. In the optimisation process,  $S_{RF}$  is adopted to measure the relative SNR improvements achieved by using different RF coil designs.

Until now, most studies have utilised simple analytical approach to estimate the SNR improvement when adopting cryogenic probes[15]. These approaches tend to lead to an inaccurate approximation of sample noise in small animal studies since  $R_{sample}$  varies a lot with characteristic sizes, conductivity geometry and magnetic field strength [16]. The theoretical solution also

neglects  $B_1$  field attenuation effect with increasing distance through the sample which must be accounted for to avoid SNR overestimation [17].

In this study, the coil size was optimised to produce the best SNR in three different areas of mouse anatomy: brain, hind legs and liver. Among these sites, the mouse brain represents a small sample loading situation, while the liver and legs represents heavy loading situations. This is particularly true in the case of the liver, which is buried at about 7 mm below the mouse body surface, the expected SNR gain will reduce with  $B_1$  field attenuation at this image depth. The finite-difference time-domain (FDTD) technique (using xFDTD from Remcom. Inc, PA) was adopted to analyse the coil's SNR performance and which offers the flexibility to study realistic small animal models, complex RF element design and metal material properties. The anatomically detailed FDTD grid of a 28g nude normal male mouse model was created by first retrieving pixels from 206 coronal images of a "digimouse" atlas (<http://neuroimage.usc.edu/Digimouse.html>) with 0.1 mm resolution, and transforming these segmented images into a 3D grid of Yee cell cubes with tissue electrical characteristics taken from ... . The simulated geometry is shown in Fig. 1 where a circular loop coil was located 1.5 mm above the mouse model to accommodate the cryogenic thermal insulation imposed by the new cryostat design. In the simulation the loop is a 3 mm thick copper wire, tuned to the desired 128 MHz for a 3T MRI scanner by one lumped element capacitor. Two conductivities  $\sigma_{293K} = 4.5 \times 10^7$  S/m and  $\sigma_{110K} = 2 \times 10^8$  S/m were used for copper at room temperature (RT = 293K) and cryogenic temperature (CT = 110 K) respectively [18]. For comparison purposes, a lossless coil made from perfect conductor (PEC) with the same coil geometry was also simulated to determine the ultimate SNR gain that could be achieved by reducing  $R_{coil}$  to its theoretical minimum. A sinusoidal current source with frequency of 128 MHz was applied as a driving port. Once the steady state of the EM evolution was obtained, the normalized transverse field  $B_1$  information was computed by exporting  $B_1$  for each grid inside the targeted imaging area, and the coil resistance  $R_{coil}$  was computed from the real part of the input impedances when the coil was first placed inside free space without mouse loading. Then a second simulation was performed where the same RF coil was positioned at targeted imaging area of the mouse model. The input impedance from this simulation was the total equivalent resistances of the receiver system,  $R_{eq}$  with the  $R_{coil}$  information obtained from the previous simulation. Then  $R_{sample}$  can be calculated from eqn (3) as:  $R_{sample} = R_{eq} - R_{coil}$ . In eqn (3), sample temperature coefficient,  $T_{sample}$ , was assumed to be 310 K, RF coil temperature coefficient at RT,  $T_{coil,RT}$  was 297 K and

$T_{coil,CT}$  was chosen to be 120 K since this is the final cooled down temperature achieved by the new cryostat design as described below .

Figure 2 shows the normalized  $S_{RF}$  at the middle slice of three targeted image areas for a series of loop radii  $r$  (varies from 0.2 cm to 4 cm) made from three different materials (copper coil at RT: RT-Copper, copper coil at CT: Cryo-Copper and a perfect lossless coil). For easy visualisation and comparison, the  $S_{RF}$  values for different coils are normalized to the maximum  $S_{RF}$  achieved by that of RT-Copper. Fig. 2 suggests that using the CT-Copper coil with optimum coil size should improve SNR performance of MR images by a factor of 2 over those of RT-Copper coil for light sample loading effects. For heavy sample loading applications, the advantage for such a coil is reduced by 22% to a 1.56 fold SNR gain. In our simulation, when the perfect conductor is adopted, the SNR gain can be further improved by 4.58 and 2.72 fold against these obtained from the CT-Coil for light and heavy sample loading situations respectively.

For the lossless coil where  $R_s \gg R_c$ , the SNR increases with the decrease of the coil size. Therefore the optimum lossless coil size is 0.4 cm. whereas for the CT-Copper coil, this size increases to 1.6~2 cm. This trend reversal is due to the fact that  $R_{coil}$  becomes dominant. When  $R_{coil}$  is added, the optimal diameter changes, and the SNR realized is less than would be achieved with lossless coils. Since the SNR variations for coil sizes between 1.6 to 2 cm are minimal, a 2 cm coil size is chosen as the optimum CT-Copper coil size for general small animal imaging applications due to its better overall  $B_1$  field penetration and hence FOV.

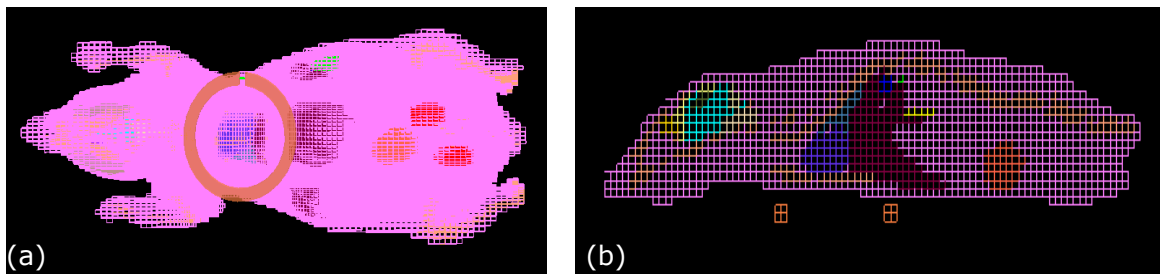


Figure 1: (a) The top view of the EM simulation setup, where a 2 cm circular copper coil is positioned 1.5 mm away from the 1 mm-resolution mouse model. Different conductivities for copper at RT and CT temperatures are applied to simulate the  $S_{RF}$  enhancement by cooling the RF coil. The detailed coil circuit is removed from the above figure to allow better visualization of the setup. (b) Side view of the EM simulation.

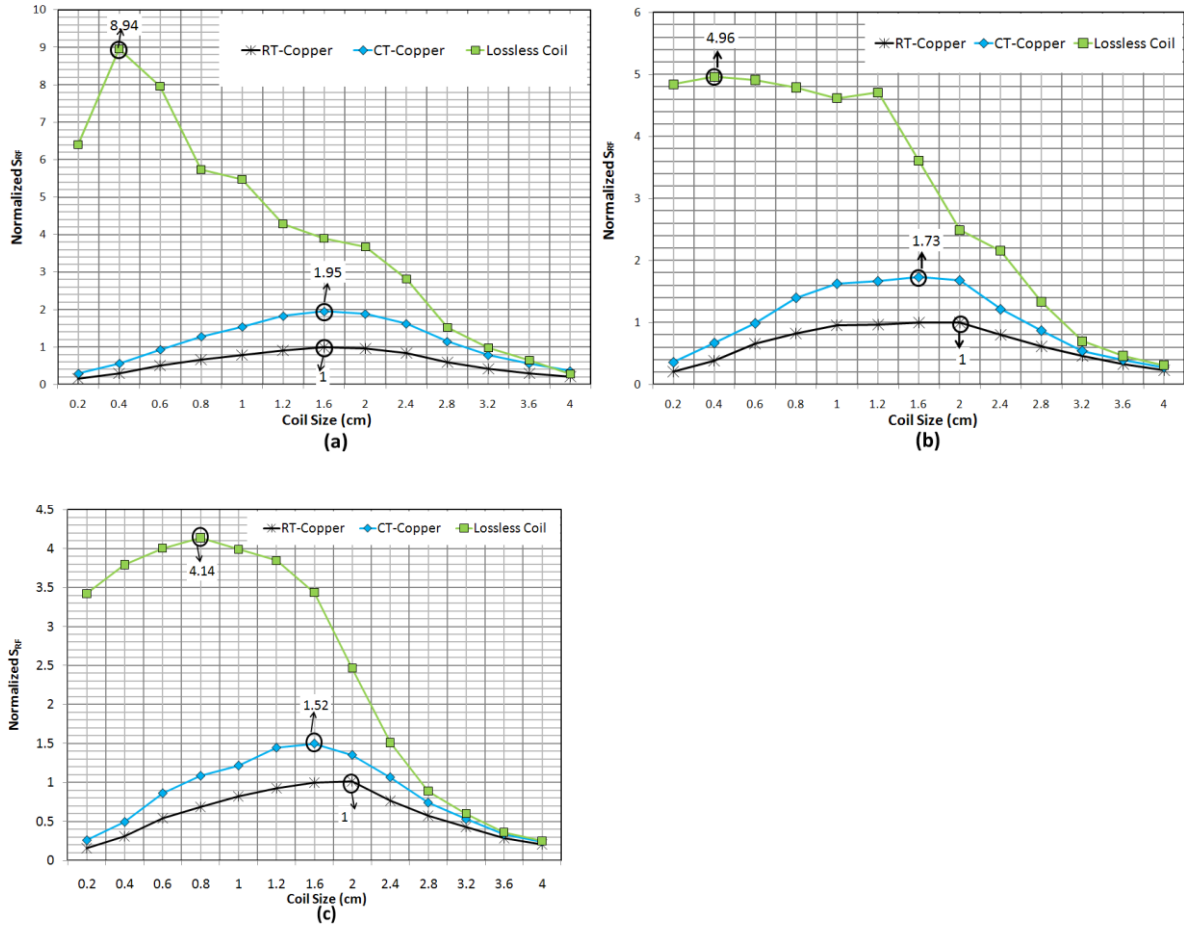
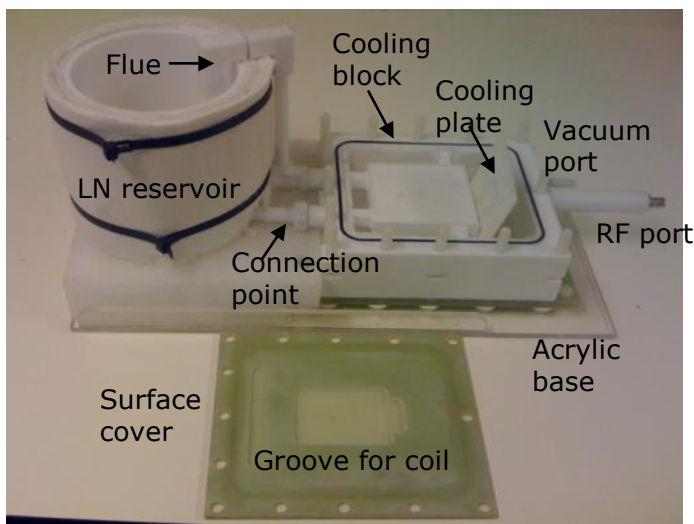


Figure 2: Normalized  $S_{RF}$  distributions at middle slices of three targeted image areas: (a) Brain, (b) hind legs, (c) liver, for a series of loop radii  $r$  made from three different materials (copper coil at RT: RT-Copper, copper coil at CT: CT-Copper and perfect conductor: lossless coil). For easy visualisation and comparison, the  $S_{RF}$  values for different coils are normalized to the maximum  $S_{RF}$  achieved by that of RT-Copper.

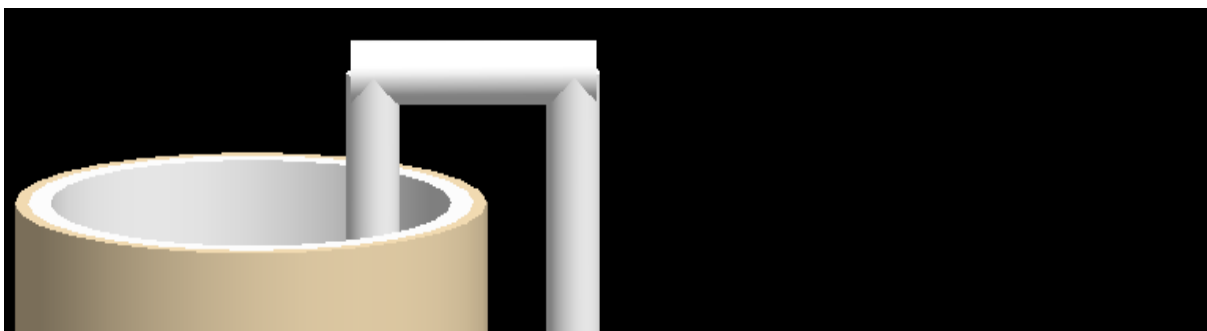
## (2) Cryostat Design:

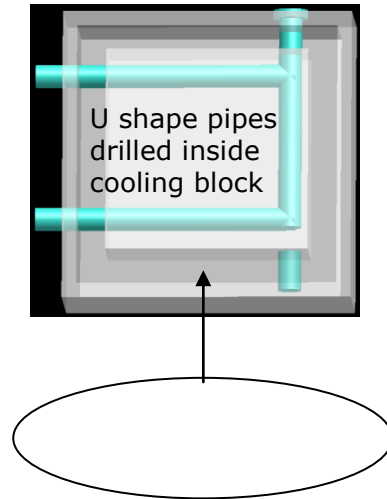
This cryostat design features a large lateral surface area for easy access, positioning and imaging of small rodents as shown in Fig. 3. The rectangular cooling unit was crafted from a 10 × 10 cm PTFE block. Three pipes were drilled inside the block to form a U-shape path for LN<sub>2</sub> circulation as shown in Fig. 3(b). The input pipe 1 was connected to the base of the LN<sub>2</sub> reservoir and the output pipe 2 is used for circulating N<sub>2</sub> back to the LN<sub>2</sub> dewar. The pressure difference between the LN<sub>2</sub> bath inside the reservoir and that inside cooling unit forces LN<sub>2</sub> flow through in the cooling unit. A 5 × 5 × 0.05 cm alumina plate was mounted above the PTFE block as a method of ensuring a uniform cooling for the RF coil. The vacuum around the cooling block was actively maintained by an oil-diffusion pump (Edwards RV5 Rotary Vane Pump, Edwards Vacuum, West Sussex, UK). The

top surface of the cryostat was made from 5 mm G10 material for its better material strength under high pressure condition. An O-ring was applied at the interface of surface cover and cooling unit to improve its vacuum insulation. A 3.5 mm thick small rectangular groove was made on the surface cover to accommodate the RF coil positioned above the alumina cold head. Therefore the overall separation distance between the nearest point of the sample and RF coil is 1.5 mm. This separation distance is similar to that of other conventional RF coils at room temperature. Since the whole cooling block for LN<sub>2</sub> circulation is made entirely from one PTFE block, the possibilities for leaking of the LN<sub>2</sub> circulating inside cooling block is greatly reduced. After cooling the unit by LN<sub>2</sub> for 45 minutes, the coil reaches a stable temperature around 120 K. Due to the high strength of the G10 material of the lateral area a vacuum pressure of 0.5 mbar pressure can be used without shape distortion of the surface. The vacuum performance was monitored by pressure meter and its thermal performance was determined by a thermocouple (although the latter was not used for imaging tests due to magnetic field effects and was removed). During a one hour imaging experiment, 1 litre of LN<sub>2</sub> was able to maintain this low temperature with only 1K thermal variation, and same level of high-vacuum (0.8 mbar) was achieved. LN<sub>2</sub> boil-off was estimated at 4 cm<sup>3</sup>/min, which allowed for 2 hours of operation before a refill. Therefore for most imaging experiments, no LN<sub>2</sub> refill or additional LN<sub>2</sub> pump is required.



(a)





(b)

Figure 3 (a): Structure of the cryostat. It has a large lateral surface area for small animal imaging. Since the cooling block is crafted from a whole piece of PTFE material, the LN<sub>2</sub> leakage is greatly reduced. (b) Illustration of the cryostat. The inset shows the pipes to circulate LN<sub>2</sub> are directly drilled inside the PTFE block. Blanking plugs were inserted to close off the drill holes.

### (3) Coil Circuit Design and its Q Factor

Before performing imaging experiments, the best way to characterise the quality of the RF coil itself is by measuring its Q factor as:

$$Q = \omega L / R_{eq} \quad (4)$$

Where  $\omega$  is the resonant frequency of the MR scanner, L is the inductance of the RF coil. To validate the accuracy of EM simulations, the expected SNR gains for the CT-Copper coil loaded with a mouse model obtained from simulation are compared with these from experimental measurements.

From our previous study, a 2 cm copper coil is chosen as a suitable coil size for small animal imaging applications, therefore a copper loop with inner diameter  $d = 2$  cm was built in house. In

order to improve the homogeneity of the MR imaging and also for the RF safety reason, the volume body coil on the MR scanner was used as a transmit coil, and the CT-Copper coil was used as receiver. An active decoupling circuit was added to the tuned and matched coil as shown in Fig. 4. The coil is inductively matched to approximately 50 Ohms. The impedance of the coil changes slightly during the cooling process due to the reduced  $R_{coil}$  and deformed matching inductor under high vacuum condition. Therefore a flexible fine-matching circuit outside the cryostat is highly desirable. In our circuit design, part of the matching circuit was moved outside the cryostat by incorporating a short transmission line in the circuit. The tuning was adjusted to compensate the frequency shift and matching when the RF coil is cooled down. The use of inductive series matching allows the PIN diode bias current to flow and hence reduces component count within the cryostat.

The Q factors of the coil inside the cryostat were experimentally measured with an HP 4395A network analyzer (Agilent, Palo Alto, CA, USA) at both RT and CT [19]. Q factors were measured for the unloaded case as well as for the coil loaded with different imaging areas of mouse: brain, liver and hind legs.

Subsequently, the expected gain in SNR between coils at two temperatures was estimated according to [20]:

$$\frac{SNR_{CT}}{SNR_{RT}} = \sqrt{\frac{RT \cdot Q_{unloaded,RT}^{-1} + RT \cdot Q_{sample}^{-1}}{CT \cdot Q_{unloaded,CT}^{-1} + RT \cdot Q_{sample}^{-1}}} \quad (5)$$

With  $Q_{sample}$  given as:

$$Q_{sample}^{-1} = Q_{loaded}^{-1} - Q_{unloaded}^{-1} \quad (6)$$

For the RT-Copper coil, the difference between the loaded and unloaded Q values was less than 10%, and  $Q_{sample}$  cannot be reliably obtained with regard to the accuracy of the measurement. Therefore  $Q_{sample}$  value obtained from the CT-Copper coil is also applied to the RT-Copper coil,

assuming the sample temperature and status did not change between experiments with RF coils at two different temperatures.

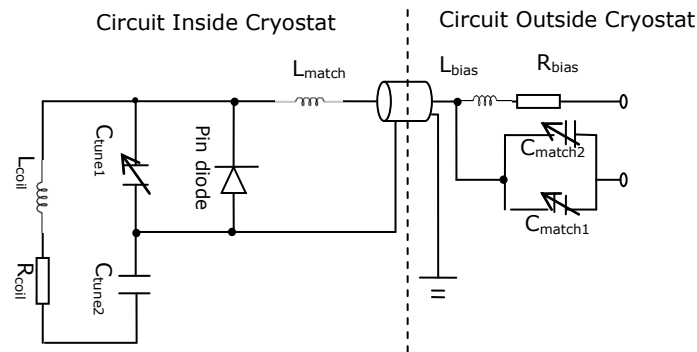


Figure 4: Schematic circuit of the 2-cm-diameter receive coil for 3T MR imaging. Two tuning capacitors are used to prevent electric field concentration and their values are  $C_{tune1} = C_{tune2} = 54$  pF. Active decoupling and inductive matching techniques are adopted, where the pin diode model is MA4P1250YO72 (M/A-COM USA), and  $L_{match}$  is a 3 mm conductor coil made from 21 turns. The fine-adjustment circuit is moved outside the cryostat via a short transmission line for extra degree of freedom in matching., where  $R_{bias} = 100$  Ohms,  $L_{bias} \gg L_{match}$  and  $C_{match1}$  and  $C_{match2}$  are parallel trimmer capacitors with a capacitance range from 5 to 30 pF.

#### (4) Image Experiment:

For comparison purpose, image experiments were first performed by using the RF coil at RT. Then the LN<sub>2</sub> reservoir was filled with LN<sub>2</sub>. After 45 minutes the coil achieved a stable temperature of around 120 K. Then the CT-copper coil was again matched to 50 Ohms by using the fine matching circuit outside the cryostat. The cryostat, still connected to the vacuum pump, was repositioned inside the scanner. Each MRI measurement of the respective image object was repeated three

times to assess reproducibility. To illustrate the potential of the coil for both *in-vitro* and *in-vivo* measurements, images were obtained on a Phillips Medical Systems Achieva 3-T whole-body scanner (Philips, Best, The Netherlands). The scanner was equipped with Dual Quasar Gradients (slewrate 200 mT/m/ms, maximal gradient strength 80 mT/m). Since this cryostat has a flat lateral surface area for small animal imaging, samples are directly positioned above the RF coil surface cover to ensure fair SNR measurements.

All animal experiments complied with the regulations of institutional animal care and use committee. A nude mouse of about 30 g were investigated under anaesthesia induced by an intraperitoneal injection of 200 mL of diluted (1/5) pentobarbital (SanofiSynthelabo Laboratory, Paris, France). To maintain the physiological activity of the mouse, its body temperature was measured by a rectal temperature probe (MLT415, ADInstruments, Spechbach, Germany). A heat module (manufacturer) is placed near to the mouse head to blow warm air and maintain a consistent temperature inside the magnet bore. Immediately after three hours imaging experiments, the mouse was euthanized with an intraperitoneal injection of a pentobarbital overdose. A total of three different anatomical sites (brain, liver, leg) were investigated. These examples were chosen to cover a representative range of *in-vivo* or *in-vitro* experiments which may have cryogenic coil applications. In order to demonstrate the robustness of the CT-Copper coil for *in-vivo* imaging applications, several widely use pulse sequences for mouse imaging were applied as shown in Table 1. MR images were acquired for coil at two temperatures using identical settings and the same imaging protocols.

A multi-slice 2D Turbo-field echo (2D-MSTFE) protocol was applied to the mouse brain image. The benefit of this technique is its fast acquisition time where  $t_{acq} = 3.5$  minutes, therefore it is suitable for small animal neuro imaging. Then a 3-D Turbo spin echo (3D-TSE) with an in-plane resolution of 100  $\mu\text{m}$  was tested. One anticipated applications of this technique involves small lesion structure assessment inside the brain by using this T2 weighted image technique [21].

An example of considerable clinical interest for the mouse's hind leg is imaging and analysis of lymph node, currently possible at a resolution of  $80 \times 80 \times 100 \text{ mm}^3$ . The inguinal lymph nodes at the hind legs of mouse are pair of tiny circular ball-shaped organs, usually 1 mm in diameter. Inguinal lymph nodes have clinical significance as they become inflamed or enlarged in various

conditions, such as life-threatening cancer diseases. High resolution MRI imaging technique is thus required to aid the cancer staging, which decides the treatment to be employed, and for determining the prognosis [22]. In our study, 3D-TFE and 3D-TSE with parameters listed in Table 3 are applied to obtain the lymph nodes images.

Finally, the mouse under anaesthesia was euthanized after 3 hours of image time (when the effect of anaesthesia almost expired) to obtain some post-mortem mouse liver images. For SNR measurement of mouse liver image, the experiments were performed within twenty minutes after its post-mortem to ensure that no differential desiccation or post-mortem changes in T1/T2 had occurred between experiments.

Image Sites	Protocols	TR/TE (ms)	BW (Hz/Pixel)	MD	FOV (mm)	$t_{acq}$ (minute)	flip angle (degree)
Brain	2D-MSTFE	36/18	34	152×150	18×18	3.45	25°
	3D-TSE	729/22	102	152×150×20	18×18×8	7.3	90°
Hind Legs	3D-TFE	50/12	134	232×231×20	35×35×8	6.05	25°
	3D-TSE	1100/12	360	480×480×20	45×45×8	8.2	90°
Liver	3D-TFE	50/12	134	232×231×20	35×35×8	6.05	25°
	T2W-TSE	3000/20	173	176×174	35×35	2.57	90°

Table 1: Parameters of scan Protocols to Image the Different Mouse Sites

(5) SNR measurements:

Performance of the RF probe at RT and CT are analyzed and compared by measuring the SNR of acquired MR images. The signal intensity,  $S_{mean}$ , is evaluated as the mean intensity value of an ROI selection across the centre of the image which corresponds to the centre of the RF coil. The noise value,  $S_{SD}$ , is evaluated by measuring the standard deviation of the signal in the background area. The SNR is then calculated as  $S_{mean}$  divided by  $S_{SD}$ , and these two parameters are obtained from three repeated measurements [23]. With the aid of medical image analysis software such as **ImageJ** and **MRCro**, the same ROI are selected and evaluated. Comparison slices are taken from

the same plane for all measurements. Subsequently, the SNR is calculated for coils at different temperatures and the relative gain in SNR between two coils is given as the ratio of their respective SNR. To evaluate the SNR across the whole MR image slice, the SNR map, where average signal intensity  $S_{\text{mean}}$  divided by the average noise level, are also plotted [24].

## **Results:**

### (1) Coil Circuit Design and its Q Factor

The experimentally measured Q factors of the RF coil at both CT and RT temperatures in loaded and unloaded situations are summarised in Table 2. The unloaded quality factor of the probe at CT is 210. A similar measurement for the same coil at RT yielded Q around 140. Therefore the Q factor is enhanced by 50% by cooling the RF coil. The expected SNR gain for the RF coil at two temperatures, derived from eqns (5)-(6) based on these measured quality factors, are also reported in Table 2. This SNR gain calculation is based on the assumption that the same  $B_1$  field available to both the RT-Copper coil and CT-Copper coil and thus the SNR gain can be determined by the ratio of the respective Johnson noise terms. For the light loading cases, such as mouse brain imaging, the expected SNR gain from a 2 cm RF coil at RT and CT is around 1.85 fold. As expected, the SNR gain decreases to 1.79 when the RF coil is loaded with mouse hind legs. While for liver area, the gain is dropped to 1.63 folds. The SNR gains determined by EM simulation are also listed in Table 2 for comparison, with the difference between results obtained from EM simulations and experiments ranging from 3 to 6%.

### (2) Small Animal Imaging

*In-vivo* mouse images acquired with the RF coil at two different temperatures following the protocols given in Table 1 are displayed in figures 5 - 12. Before performing comprehensive SNR comparisons between the CT-Coil and RT-Coil, SNR performances of these two setups need to be characterised against a commercially available surface coil with similar dimension to ensure fair comparisons. A 23 mm microscopic surface coil (Philips) is used as a benchmark and its technical details can be obtained from the manufacturer. The SNR plots of the midline of the MR mouse

brain image obtained by using the 2D-MSTFE protocol with three coils were plotted in Fig. 5. Among these three coils, the CT-Coil achieved substantial SNR enhancement compared with the other two coils operated at RT. For the RT-Coil and Commercial Coil, their SNR performances were almost identical despite the sharp spike at the depth 1.79-2.68 mm from that of Commercial Coil. This is due to the fact that the animal positioning was changed for two different coils. Since the RT-Coil achieves similar SNR performance compared with an optimum surface coil with similar dimension, the SNR comparisons were made only between the RT-Coil and CT-Coil for the following experiments for simplicity. Images of the mouse brain obtained with Brain 2D-MSTFE protocol at about the same anatomical position by using CT-Copper and RT-Copper coils are presented in Fig. 6(a) and (b). Figure 7 shows the resulting SNR maps of mouse brain images obtained from the 3D-TSE protocol with these two coils. For all sequences the use of the CT-Copper coil provides better image quality, i.e., higher SNR values and clearer anatomical details, as compared with its identical counterpart at RT. In Fig. 6, detailed brain structures such as the corpus callosum, the hippocampus, the D3V (dorsal 3<sup>rd</sup> ventricles), the PH (posterior hypothalamic area), ArcLP(arcuate nucleus of hypothalamus), the division between IC (interior capsule) and EC (exterior capsule) are better visualized by using this setup. An SNR of about 20 allows clear discrimination of inner structures of hippocampus area, such as CA1 and CA2. In the images of the mouse brain, the signal-to-noise ratio increased by a factor 2 in the EC, 1.9 in the hippocampus, 1.95 in the central thalamus, and 1.75 in the hypothalamus using the CT-Copper coil relative to the same points in the brain images acquired with the RT-Copper coil. These results are similar to the value of 1.95 predicted from simulation results as shown in Fig. 2(a). Noticeably, the SNR gain of the cerebral cortex area is around 1.82 fold, and this improved image quality will aid the development of fMRI study for small animals. Since the FOV from the same RF coil at different temperatures are about the same, the above SNR analysis shows very little dependence on measurement location across the whole MR image slice. The slight SNR gain variations between different tissues are due to the difficulty of in vivo SNR measurements, such as differences in tissue contrast and anatomical registrations on the measurement. To compare the general SNR gain across the whole slice of image, SNR maps of about the same image slice obtained at two temperatures are also produced in Fig. 7. To generate those maps, we defined SNR of each pixel as the ratio of its signal intensity over the standard deviation of an ROI on the background. The SNR maps indicate the substantial SNR enhancement around 1.93 fold along the whole slice is

achieved with the CT-Copper coil. It is found that the SNR gain has little dependence on different pulse sequences, and the difference between SNR gains for SE and GE sequences is within 5%.

Lymph node images obtained with 3D-TFE and 3D-TSE protocols are demonstrated in Fig. 8 and 9 respectively. The 1.12 cm in diameter lymph nodes for both hind legs are already well delimited with an SNR of 21.2 at a 4.5 mm depth inside the mouse body. The image in Fig. 8(a) and 9(a) obtained with CT-Copper coil shows a substantial difference in the observed SNR compared with Fig. 8(b) and 9(b) as it reveals a clear distinction between the outer capsule of lymph node and its surrounding fat. In contrast, images obtained with RT-Copper coil shows a grainier appearance of the image which lacks contrast and details. The SNR profiles of ten pixels across the centre of the right inguinal lymph node are shown in Fig. 10. When the RF coil is cooled down to CT, SNR measured at lymph node area increased from 12.4 (for coil at RT) to 21.2 (coil at CT), an improvement of 1.7. Although 3D-TFE technique achieves a 7% higher SNR gain than that of 3D-TSE, there is no clear correlation between SNR gain and imaging protocols. Compared with the mouse brain image, the SNR gain of mouse hind leg image dropped to 1.75 fold. Two possible reasons for this SNR gain reduction are: (1) the interested ROI location is at the edge of the coil illumination area, each lymph node is around 10~11 mm from the centre of the coil; (2) the distance between the coil and ROI region is increased from 2 mm for the mouse brain image to 4.5 mm for lymph node images.

Figure 11 and 12 display in vitro image of a mouse liver obtained with 3D-TFE and T2W- TSE protocols respectively. The mouse liver was chosen to demonstrate the potential of the cryogenic coil as an imaging tool to study the contrast uptake dynamics where quick scan time and high resolution image are required. This protocol achieves a high resolution around  $100 \times 100 \times 400 \mu\text{m}^3$  voxels at time per image of 6.12 minutes. For images obtained with the CT-Copper coil, the SNR was 28.57, and for the RT-Copper coil, the SNR is reduced to 17.85, yielding an advantage of 1.6 by adopting the cryogenic coil technique. The gain measured in these images was slightly less than that seen for the other sites of mouse, and it is consistent with the EM simulation where the coil sensitivity is reduced by greater sample loading of small animal's upper body. Compared with Table 2, this measured SNR gain is 1.25% lower than the expected SNR gain obtained from Q factor measurements. The slight differences between the measurements and experiments are due to the natural movements of the small animal. Note in Fig. 11 that the multiple lesions that are the

thickness of only 3–4 cells are much better visualized by using the CT-Copper coil. In Fig. 12, the Hepatic Portal Vein can be clearly seen by using the T2W-TSE imaging technique.

Loading situation	Measured Q factor		Expected SNR gain	Simulated SNR gain	Relative Error (Between simulation and experiments)
	CT-Copper	RT-Copper			
Unloaded	210	140	N/A	N/A	N/A
Mouse Head	202	136	1.8479	1.95	5.24%
Mouse Hind Legs	195	134	1.7948	1.73	3.57%
Mouse Liver	170	121	1.6297	1.52	6.73%

Table 2: Evaluation of the coil quality in terms of its Q factors and expected SNR gains when loaded by three anatomical sites of the mouse in vivo.

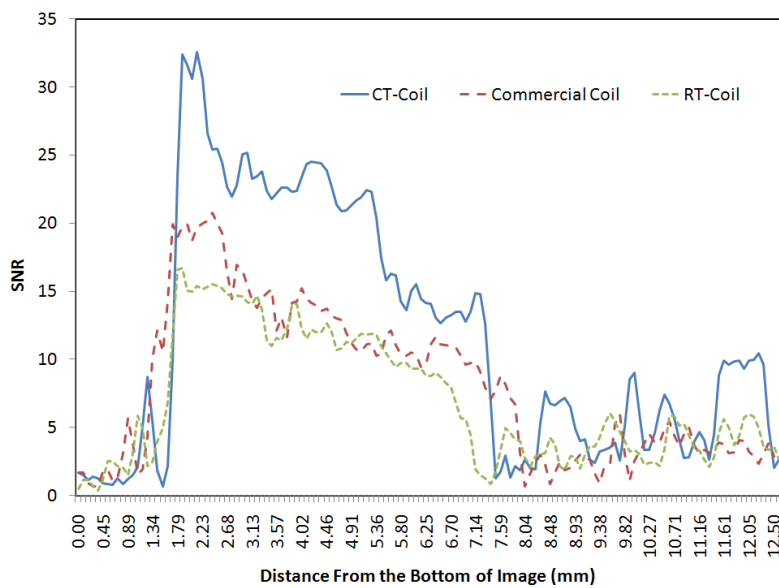


Figure 5: Comparison of

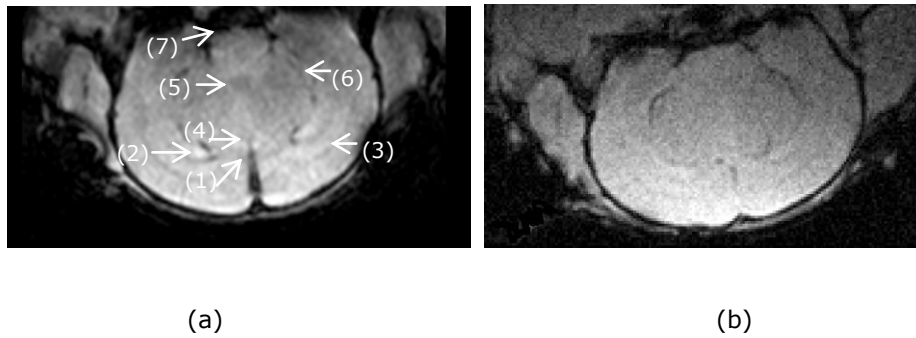


Figure 6: In vivo axial images of the mouse brain. Images were acquired using the 2D-MSTFE. (a) is obtained with the CT-Copper coil, and (b) is obtained with the RT-Copper coil. The arrows indicate different tissues where (1) corpus callosum, (2) hippocampus, (3) Internal capsule, (4) D3V (dorsal 3rd ventricles), (5) PH (posterior hypothalamic area), (6) EC (external capsule), (7) ArcLP (arcuate nucleus of hypothalamus).

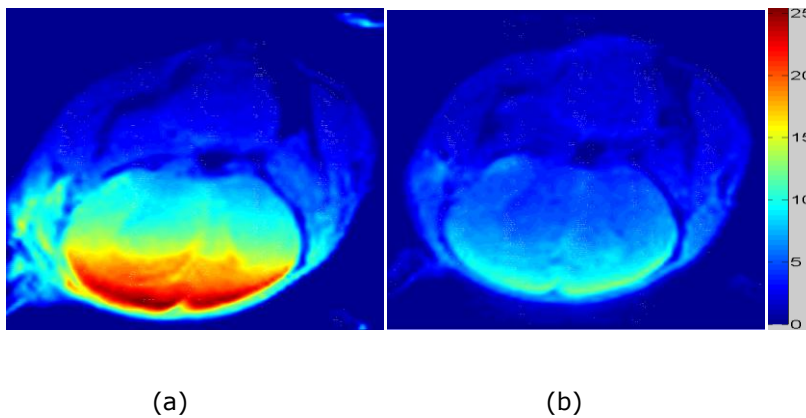
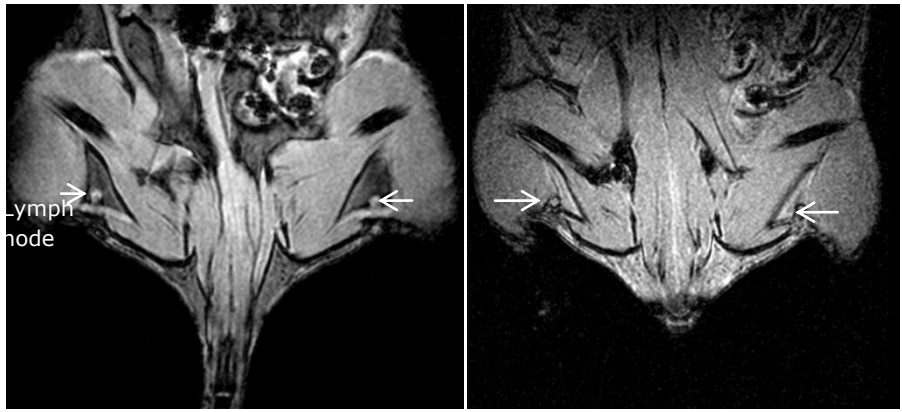


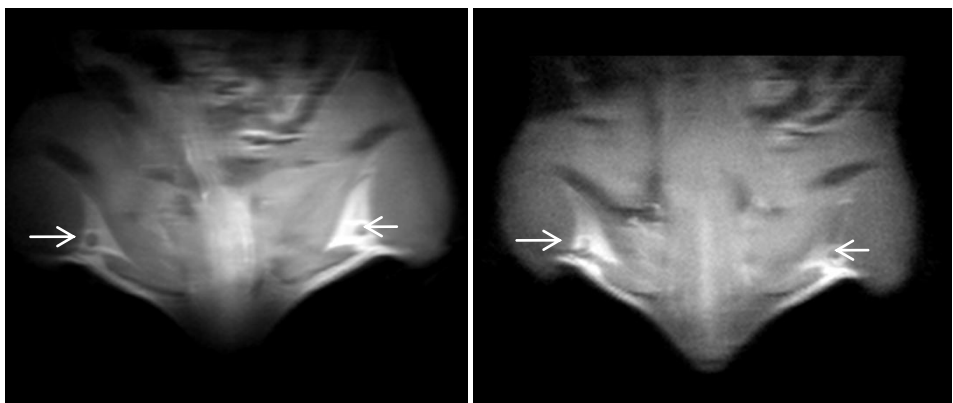
Figure 7: SNR maps of the mouse brain acquired from 3D-TSE protocol. (a) is obtained with the CT-Copper coil and (b) is from the RT-Copper coil. Note that the SNR magnitude from (a) is doubled compared with that from (b).



(a)

(b)

Figure 8: In vivo coronal slice of the mouse hind legs. The image has been acquired with 3D-TFE protocol. (a) is obtained with the CT-Copper coil, and (b) is obtained with the RT-Copper coil. The arrows indicate the interested ROI region for this study, the lymph node.



(a)

(b)

Figure 9: In vivo coronal slice of the mouse hind legs. The image has been acquired with 3D-TSE protocol. (a) is obtained with the CT-Copper coil, and (b) is obtained with the RT-Copper coil. The arrows indicate the interested ROI region for this study, the lymph node.

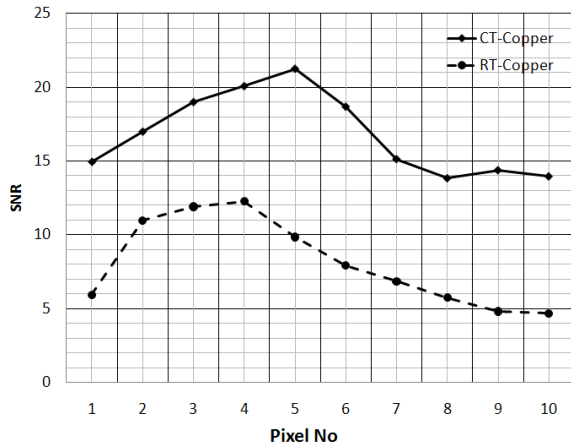


Figure 10: The SNR profiles of ten pixels across the centre of the right inguinal lymph node from Fig. 7 obtained from CT-Copper and RT-Copper coils. An improvement of 1.7 fold is achieved by cooling down the coil to CT.

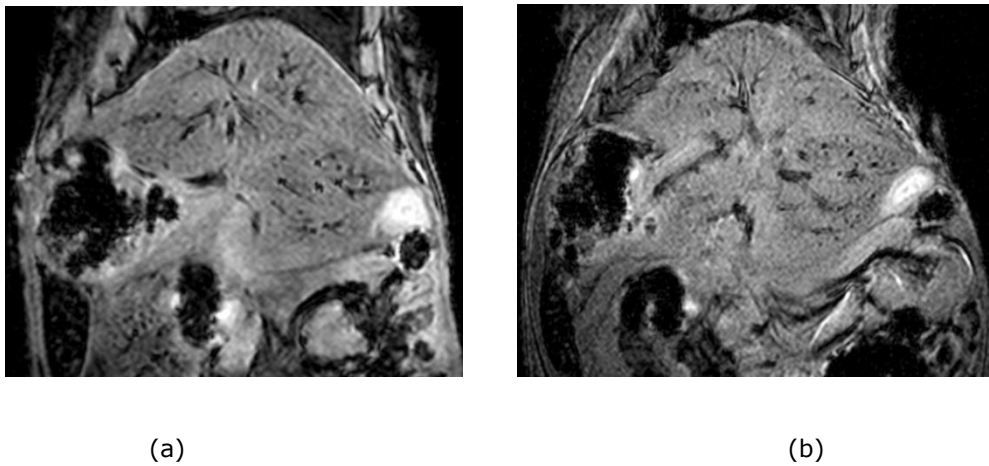
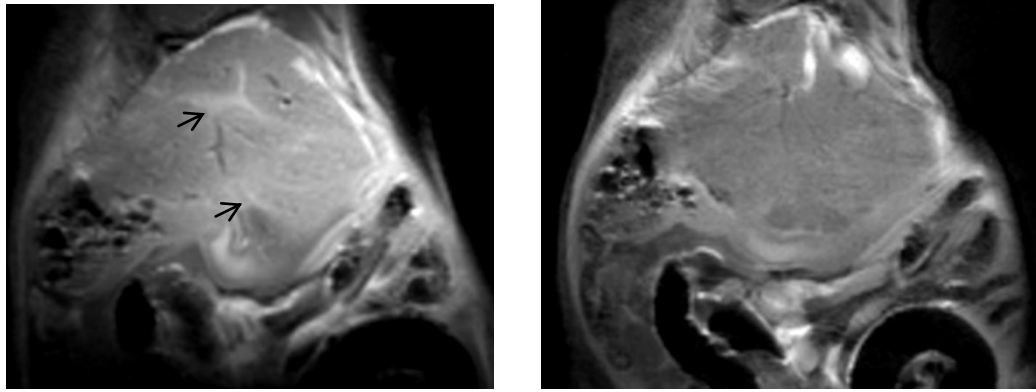


Figure 11: Coronal slices of mouse liver images acquired with 3D-TFE protocol. (a) is obtained with the CT-Copper coil, and (b) is obtained with the RT-Copper coil. With this GE imaging technique, small lesions can be clearly identified in Fig. 10(a) with the Cryo-Copper coil.



(a)

(b)

Figure 12: Coronal slices of mouse liver images acquired with T2W-TSE protocol. (a) is obtained with the CT-Copper coil, and (b) is obtained with the RT-Copper coil. In Fig. 11(a), the Hepatic Portal Vein indicated by arrows can be clearly delimited by using the Cryo-Copper coil.

### Discussion:

Until now, most clinical scanner compatible cryogenic coils have been designed for magnetic fields lower than 1.5T. In the sample dominant regime, improper choice of coil size will result in  $R_{\text{sample}} \gg R_{\text{coil}}$ , and only marginal SNR enhancement will be gained by adopting cryogenic coil. In this paper, the possible SNR gain achieved by adopting cryogenic coil at 3T is first studied by EM simulation. In the EM simulation, only two major noise sources ( $R_{\text{sample}}$  and  $R_{\text{coil}}$ ) were considered while other losses introduced by electronic components and solder joint connections were neglected. This is because for RF coil made from copper material, the major coil noise still rises from the Johnson noise of the metal [25].

In our design, the cryostat body and cooling block is made from a single piece of PTFE material, therefore it greatly improves the vacuum integrity and insulation capability. However, the temperature drop achieved by this cryostat is 180 K, about 20% higher than that of LN<sub>2</sub> itself ( i.e. 120 K). This is due to the thermal losses of the PTFE material. In the future, when the cryogenic temperature can be further improved, the SNR gain can be enhanced further by lowering the cryogenic coil temperature. From the simulation, the SNR gain achieved by cooling the copper coil to 80 K would be around 2.7, assuming an increase of conductivity by a factor of 2.6 [30].

Compared with the SNR gain achieved by adopting the current setup, the SNR gain can be improved by 38% by adopting more thermally conductive material to build the cryostat. The construction used here is simple and effective and merely serves as proof of principle. In future cryostats with better thermal performance and with a reasonable material strength can be constructed by using ceramic material [1]. Such designs would allow greater proximity of the coil to the tissue, important for very small coils. Because the good thermal insulation performance of this cryostat, typical problems associated with this LN<sub>2</sub> coolant type of cryostat, such as quick boil-off and bubbling of LN<sub>2</sub>, thermal instabilities and RF fluctuations due to different dielectric constants between liquid and gas phases have not been observed. For our experiment, data of temperature variation were acquired by using a thermocouple inside the cryostat, and there was minimal temperature change during 2 hour imaging time. A stable electrical performance in terms of Q factor and resonant frequency were obtained by using this CT-Copper coil setup.

In this paper, we proposed the first cryogenic receive-only coil with active decoupling circuit. The whole body volume coil is adopted as transmit coil to achieve uniform flip angle patterns across the MR image. In this report, the SE pulse sequence is successfully applied to several mouse anatomical sites. Compared with the GE pulse sequence, the SE image protocol requires uniform tip angle to achieve 180 degree magnetisation inversion. Therefore the SE pulse is rarely adopted by other cryogenic coil techniques [26].

In the past, several reports suggested that an average SNR gain around two-fold can be achieved for MR images by cooling down the RF copper coil to cryogenic temperatures. However the separation between the cryogenic coil and sample is usually bigger than 3 mm [27], and this distance adversely influenced the MR image quality since it degrades the filling factor which depends on the proximity of the actual coil structure to the sample. In this paper, this distance is reduced to 1.5 mm.

For the MR image experiments, micron scale high resolution MR images of small animal were obtained on a clinical whole body scanner by using this engineering solution. The two-fold SNR gain achieved by this coil should provide great benefits to high-resolution medical imaging in three ways: (1) An SNR gain around 2 folds translates into reduction of linear voxel dimensions to 71% of the original value for 2D and 80% for 3D imaging. (2) data acquisition time and number of

average can be reduced by a factor of 4 or even more, since SNR varies as the square root of the number of signal averages. (3) image quality achieved at 3T by adopting cryogenic coil provides an SNR similar to that of a normal RF coil at 6–7 T but without issues associated with higher-field MRI, such as much more expensive scanners and higher RF power depositions that increase as the square of field strength.

The SNR gain achieved by this engineering setup was also compared with those of other cryogenic copper coil setups demonstrated by other investigators. The largest gains to date were reported by Wright et al [2] who demonstrated a 2.7 gain in SNR when comparing coils of identical geometry. This value is comparable to the 2.1 gain attained with the Cryo-Copper demonstrated in this work. The better SNR performance is due to the better cooling capability of an upright LN<sub>2</sub> bath type of cryostat.

To further reduce the coil resistance, the HTS material can be adopted instead of copper material. The **loaded** Q factor of a HTS coil is usually 10 times higher compared with that obtained by using a cryogenic copper coil in similar size [1], [5]. Until now, only one group reported a 10 folds SNR gain for in-vitro phantom study by utilizing the HTS coil on a whole body 1.5T scanner [1]. However there is no report on its applications at higher field clinical scanner (3T and above). There are several difficulties faced when trying to employ such a coil at a higher magnetic field: (1) the ultimate SNR gain is limited by the performance of the superconducting material, which is adversely affected by the increased magnetic field strength. (2) Construction of array coils and three-dimensional shapes are approved to be difficult for HTS material, compared with more flexible copper coil [28]. (3) Due to the extremely high Q factor of the HTS coil, how to maintain its stable electrical performance is another issue [29]. The corresponding band pass for the HTS coil operating at high field scanner is very narrow, therefore tuning must be accurate to account for animal movements and breathing. On the other hand, any temperature drift will also change its electrical performances dramatically.

## **References:**

- [1] M. Poirier-Quinot, J. Ginefri, O. Girard, P. Robert, and L. Darrasse. Performance of a Miniature High-Temperature Superconducting (HTS) Surface Coil for In Vivo Microimaging of the Mouse in a Standard 1.5T Clinical Whole-Body Scanner. *Magn Reson Med* 2008;60:917–927.
- [2] A. C. Wright, H. K. Song, and F. W. Wehrli. In Vivo MR Micro Imaging With Conventional Radiofrequency Coils Cooled to 77°K. *Magn Reson Med* 2000;43:163–169.
- [3] P.T. Callaghan, *Principles of Nuclear Magnetic Resonance Microscopy*: Clarendon Press, Oxford; 1991.
- [4] S.E. Hurlston, W.W. Brey, S.A. Suddarth, and G.A. Johnson. A High-Temperature Superconducting Helmholtz Probe for Microscopy at 9.4 T. *Magn Reson Med* 1999; 41: 1032-1038.
- [5] L. Darrasse, J. Ginefri. Perspectives With Cryogenic RF Probes in Biomedical MRI. *Biochimie*, 2003; 85: 915-37.
- [6] J. K. Barral, N. K. Bangerter, B. S. Hu, and D. G. Nishimura, In Vivo High-Resolution Magnetic Resonance Skin Imaging at 1.5 T and 3 T. *Magn Reson Med* 2010;63:790–796.
- [7] D. Ratering, C. Baltes, J. Nordmeyer-Massner, D. Marek, and M. Rudin. Performance of a 200-MHz Cryogenic RF Probe Designed for MRI and MRS of the Murine Brain. *Magn Reson Med* 2008; 59: 1440-1447.
- [8] Q. Y. Ma, K. C. Chan, D. F. Kacher, E. Gao, M. S. Chow, K. K. Wong, H. Xu, E. S. Yang, G. S. Young, J. R. Miller, F. A. Jolesz. Superconducting RF Coils for Clinical MR Imaging at Low Field. *Academic Radiology* 2003; 10: 978-987.
- [9] H. Cheong, J. Wild, N. Alford, I. Valkov, C. Randell, M. Paley. A High Temperature Superconducting Imaging Coil for Low-Field MRI. *Concept Magn Reson* 2010; 37B: 56-64.
- [10] J. Fang, M. S. Chow, K. C. Chan, K. K. Wong, G. X. Shen, E. Gao, E. S. Yang and Q. Y. Ma, Design of Superconducting MRI Surface Coil by Using Method of Moment. *IEEE Trans. Applied Superconductivity* 2002; 12: 1823-1827.
- [11] J. Ginefri, L. Darrasse, and P. Crozat. High-Temperature Superconducting Surface Coil for In Vivo Microimaging of the Human Skin. *Magn Reson Med* 2001; 45: 376-382.

- [12] W.A. Edelstein, G.H. Glover, C.J. Hardy, R.W. Redington. The Intrinsic Signal-To-Noise Ratio in NMR Imaging. *Magn Reson Med* 1986; 3: 604–618.
- [13] J Mispelter, M. Lupu, A. Briguet. *NMR Probeheads for Biophysical and Biomedical Experiments*: Imperial College Press, London; 2006.
- [14] A. Kumar, W. A. Edelstein and P. A. Bottomley. Noise Figure Limits for Circular Loop MR Coils. *Magn Reson Med* 2009; 61: 1201–1209.
- [15] J. C. Nouls , M. G. Izenson, H. P. Greeley, G. A. Johnson, Design of a Superconducting Volume Coil for Magnetic Resonance Microscopy of The Mouse Brain. *J. Magn Reson* 2008; 191: 231–238.
- [16] W. Schnell, W. Renz, M. Vester and H. Ermert. Ultimate Signal-to-Noise-Ratio of Surface and Body Antennas for Magnetic Resonance Imaging. *IEEE Trans Anten. Prop.* 2000; 8: 418-428.
- [17] P.J. Cassidy, S. Grieve, K. Clarke, D.J. Edwards. Electromagnetic Characterisation of MR RF Coils Using the Transmission-Line Modelling Method. *Magn Reson Mat Phy, Bio and Med* 2002; 14: 20–29.
- [18] S. N. Khanna and A. Jain. Resistivity of Solid Fe, Cu, W, Nb, Ta, MO and Pd Using t Matrix. *J. Phys. F: Metal Phys.* 1974 ; 4: 1982-1986.
- [19] L. Darrasse, G. Kassab. Quick Measurement of NMR-Coil Sensitivity With a Dual-Loop Probe. *Rev Sci Instrum* 1993; 64: 1841–1844.
- [20] DI. Hoult, PC. Lauterbur. The Sensitivity of the Zeugmatographic Experiment Involving Human Samples. *J Magn Reson* 1979; 34: 425–433.
- [21] Y. Y. Jeong, D. G. Mitchell and G. A. Holland. Liver Lesion Conspicuity: T2-Weighted Breath-hold Fast Spin-Echo MR Imaging Before and After Gadolinium Enhancement—Initial Experience. *Radiology.* 2001; 219: 455-460.
- [22] E. P. Kaldjian, J. E. Gretz, A. O. Anderson, Y. Shi and S. Shaw. Spatial and Molecular Organization of Lymph Node T Cell Cortex: A Labyrinthine Cavity Bounded by An Epithelium-Like Monolayer of Fibroblastic Reticular Cells Anchored To Basement Membrane-Like Extracellular Matrix. *International Immunology* 2001; 13: 1243–1253.

[23] JR. Miller, SE. Hurlston, QY. Ma, DW. Face, DJ. Kountz, JR. MacFall, LW. Hedlund, GA, Johnson. Performance of A High-Temperature Superconducting Probe for In Vivo Microscopy at 2.0 T. *Magn Reson Med* 1999;41:72–79.

[24] M. S. Ramirez, E. Esparza-Coss, J. A. Bankson. Multiple-Mouse MRI With Multiple Arrays of Receive Coils. *Magn Reson Med* 2010; 63: 803-810.

[25] M. Poirier-Quinot, J-C Ginefri, L. Darrasse, F. Ledru, P. Fornes. Preliminary Ex-Vivo 3D Microscopy of Coronary Arteries Using a Standard 1.5T MRI Scanner and a HTS RF Probe. *MAGMA* 2005; 18: 89–95.

[26] J. Wosik, F. Wang, L. Xie, M. Strikovski, M. Kamel, K. Nesteruk, M. Bilgen, and P. A. Narayana. High-Tc Superconducting Surface Coil for 2 Tesla Magnetic Resonance Imaging of Small Animals. *IEEE Trans Applied Superconductivity* 2001; 11: 681-684.

[27] D. Bracanovic, A. A. Esmail, S. J. Penn, S. J. Webb, T. W. Button and N. M. Alford. Surface  $\text{YBa}_2\text{Cu}_3\text{O}_7$  Receive Coils for Low Field MRI. *IEEE Trans. Applied Superconductivity*, 2001; 1 I: 2422-2424.

[28] WE. Kwok, ZG. You. In Vivo MRI Using Liquid Nitrogen Cooled Phased Array Coil at 3.0 T. *Magn Reson Imaging* 2006; 24: 819–823.

[29] M. Poirier-Quinot, J-C Ginefri, P. Robert, L. Darrasse Feasibility of In Vivo Microimaging of The Mouse In A Conventional 1.5 T Body Scanner Equipped With A 12 mm HTS Surface coil. In: *Proceedings of the 12th Annual Meeting of ISMRM, Kyoto, Japan, 2004 (Abstract 1754)*.